Ash from the Toba supereruption in Lake Malawi shows no volcanic winter in East Africa at 75 ka

Christine S. Lane[a,1], Ben T. Chorn[b], and Thomas C. Johnson[b]

[a]Research Laboratory for Archaeology and the History of Art, University of Oxford, Oxford OX1 3QY, United Kingdom; and [b]Large Lakes Observatory and Department of Geological Sciences, University of Minnesota, Duluth, MN 55812

Edited by Mark H. Thiemens, University of California at San Diego, La Jolla, CA, and approved March 15, 2013 (received for review January 23, 2013)

The most explosive volcanic event of the Quaternary was the eruption of Mt. Toba, Sumatra, 75,000 y ago, which produced voluminous ash deposits found across much of the Indian Ocean, Indian Peninsula, and South China Sea. A major climatic downturn observed within the Greenland ice cores has been attributed to the cooling effects of the ash and aerosols ejected during the eruption of the Youngest Toba Tuff (YTT). These events coincided roughly with a hypothesized human genetic bottleneck, when the number of our species in Africa may have been reduced to near extinction. Some have speculated that the demise of early modern humans at that time was due in part to a dramatic climate shift triggered by the supereruption. Others have argued that environmental conditions would not have been so severe to have such an impact on our ancestors, and furthermore, that modern humans may have already expanded beyond Africa by this time. We report an observation of the YTT in Africa, recovered as a cryptotephra layer in Lake Malawi sediments, >7,000 km west of the source volcano. The YTT isochron provides an accurate and precise age estimate for the Lake Malawi paleoclimate record, which revises the chronology of past climatic events in East Africa. The YTT in Lake Malawi is not accompanied by a major change in sediment composition or evidence for substantial temperature change, implying that the eruption did not significantly impact the climate of East Africa and was not the cause of a human genetic bottleneck at that time.

The injection of ash and aerosols into the stratosphere by explosive volcanic eruptions can trigger complex climatic feedbacks, often promoting surface cooling (1–3). Voluminous ash fall deposits blanket landscapes, at least locally, smothering vegetation, blocking sunlight, and contaminating water supplies. The 75-ka (4) Youngest Toba Tuff (YTT) has been identified in sediments from the South China Sea (3) and across the Indian Ocean, some 4,500 km west of the caldera (5–7) as well as throughout India (8). The climatic impact of the Toba supereruption, estimated to have erupted between 10 and 360 times more H_2SO_4 than Pinatubo (9), has consequently been the focus of much research over the past three decades (1, 3–5, 10–16).

An exceptional sulfate spike in the Greenland Ice Sheet Project Two (GISP2) ice core record, of 6 y duration, has been correlated to the YTT (16) despite an absence of volcanic material. The spike is dated to 71.1 ± 5 ka B.P. by layer counting (16) and more recently to 74.2 ± 1.7 ka B.P. by correlation to European speleothem records (17). Recent inspection of the sulfate records from the European project for ice coring in Antarctica's dronning maud land (EDML) ice core reveals sulfate peaks that have been correlated to presumed YTT sulfate peaks in the North Greenland ice core project (NGRIP) and GISP2 ice cores; however, once again no volcanic material has been identified (18). The positions of the sulfate peaks in both northern and southern hemisphere ice cores at the start of the ~1,000 y stadial between Dansgaard-Oeschger events 19 and 20 has been widely used within climate models (9, 14) and archaeological debate (12, 13, 19) to infer that the Toba eruption triggered devastating global cooling. This "volcanic winter" (20) has been cited as one cause of a bottleneck in modern human populations that explains limited modern-day genetic diversity (10, 11), although the genetic data can as easily be explained by other, noncatastrophic factors (21). In contradiction to this theory is archaeological evidence to suggest early modern humans had already expanded beyond Africa by this time (22) and that the eruption of the YTT did not disturb the behavior of populations inhabiting peninsular India (12).

Evidence for approximately contemporaneous global cooling in sediments that do contain YTT glass shards has been found in marine core oxygen isotope records from the South China Sea (3), as have terrestrial carbon isotope and pollen records from Northern India and Bengal (23). A marine core from the Arabian Sea, however, shows no evidence for concomitant cooling (7). To date therefore, a combination of insufficient resolution in marine and terrestrial sediments bearing the YTT and a lack of YTT ash in the polar ice cores has prevented precise evaluation of the YTT's impact on global climate and hominin populations.

Here we report an observation of the YTT in Africa, recovered as a cryptotephra layer in sediments cored from Lake Malawi >7,000 km west of the source volcano in Sumatra. Lake Malawi is 600 km long, 35 km wide, and has a maximum depth of 700 m; it is the second largest and the southernmost great lake in the East African Rift Valley. The lake is anoxic below a depth of 200 m, thus the silty diatomaceous clay that accumulates in the deep basins has not been subject to bioturbation throughout much of the lake's history. The Lake Malawi Drilling Project recovered long cores from two sites in the lake in 2005 (Fig. 1) (24, 25). We have examined the upper 40 m of sediment from both sites for tephra layers (*Materials and Methods*). Based on the existing age model (24), we targeted a search for cryptotephra (subtle horizons of volcanic glass shards not visually apparent or detectable using remote sensing methods) on the depth interval of 20–40 m below lake floor (MBLF) in drill sites MAL05-1C and MAL05-2A in search of the YTT.

Results

Tephra layers in Lake Malawi sediments are derived primarily from the Rungwe Volcanic Province (RVP) to the northwest of Lake Malawi. A cryptotephra layer was found at 28.08–28.10 MBLF, with a concentration of ~3,500 glass shards per gram sediment in MAL05-1C (Fig. 2). The cryptotephra was both morphologically and chemically distinct from the tephra layers derived from the RVP. Glass shards from RVP tephra layers are typically elongate and highly vesicular, whereas this tephra is dominated by platy shards, 30–70 μm across, with concave ("bubble wall") faces and few vesicles (Fig. 3*A*). The chemical composition of this cryptotephra is enriched in silica and alkali

Author contributions: T.C.J. conceived the project; C.S.L. and T.C.J. designed the analytical procedure; C.S.L. and B.T.C. performed research; and C.S.L., B.T.C., and T.C.J. wrote the paper.

The authors declare no conflict of interest.

This article is a PNAS Direct Submission.

[1]To whom correspondence should be addressed. E-mail: Christine.Lane@rlaha.ox.ac.uk.

This article contains supporting information online at www.pnas.org/lookup/suppl/doi:10.1073/pnas.1301474110/-/DCSupplemental.

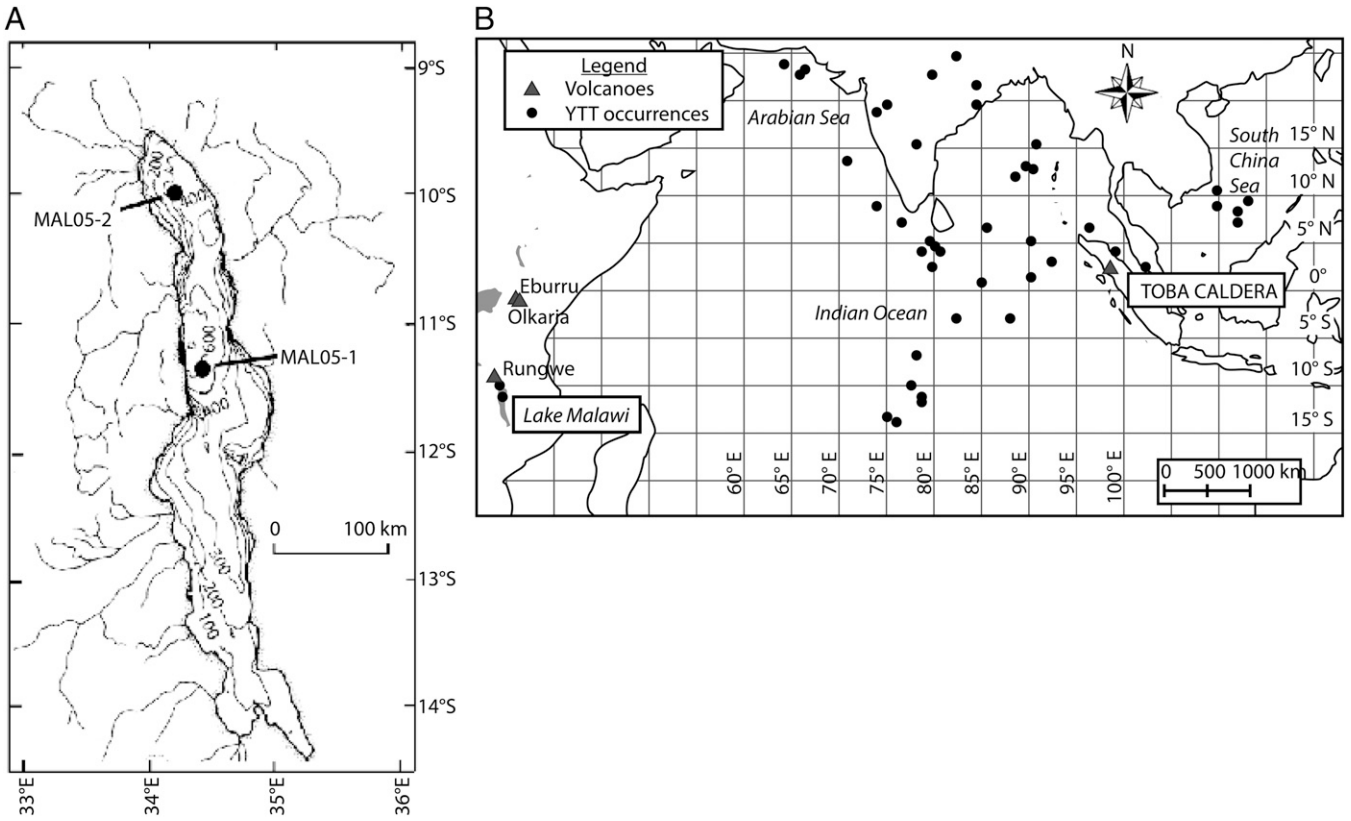

Fig. 1. Bathymetric map of Lake Malawi and overview map of YTT distribution, showing sites mentioned in the text. (*A*) Bathymetric map of Lake Malawi showing central GLAD7-MAL05-1 and northern GLAD7-MAL05-2 core locations (25). (*B*) Occurrences of the YTT across the Indian Ocean region, southern Asia, and the South China Sea (1, 3, 5–8, 12, 23). Lake Malawi, the Rungwe Volcanic Province, and other volcanoes mentioned in the text are marked.

metals and distinctly different from the RVP tephra, which are predominantly trachydacitic in composition (26), or from any other known contemporary East African rhyolitic tephra sources (27, 28) (Fig. 3*B*). Instead, the cryptotephra composition correlates to that of the 75 ka YTT (29) (Table 1 and Table S1). We subsequently found the YTT at 26.77–26.79 MBLF in drill site MAL05-2A, which confirms the existing stratigraphic correlation between the central and northern basin cores.

Discussion

Our discovery of ash from the 75 ka eruption of Toba (YTT) in Lake Malawi, ∼7,300 km from the caldera in Sumatra, increases the previously known dispersal distance of ash from this supereruption by nearly 3,000 km (Fig. 1), extending the areal coverage of this deposit to at least 2×10^7 km^2. A recent model suggests that transportation of the Toba ash westward over Africa was most likely by coignimbrite processes (30). YTT dispersal may have further exceeded the current estimates, and we predict that further cryptotephra investigations will recover YTT from other sites in Africa.

Recent dating of the YTT by high precision ^{40}Ar/^{39}Ar dating of near-vent sanidine phenocrysts has generated two partially overlapping age estimates: 75.0 ± 0.9 ka (4) and 73.88 ± 0.32 ka (17). The difference between these ages is attributed to the standards and optimization models used in the ^{40}Ar/^{39}Ar age calibration process (4). Here we take the age of 75.0 ± 0.9 ka B.P., which was calculated using the currently best constrained ^{40}Ar/^{39}Ar optimization model (4, 31) as the most robust age for the YTT, and import it into a revised Bayesian age model for the Lake Malawi central basin core, MAL05-1C (Fig. 4). The resulting model differs from the previously published age-depth model (24) by ∼10 ka at a depth of 28.10 MBLF (*Materials and Methods*). The revised age–depth model reveals that the published age estimates based on some previously identified paleomagnetic events and optically stimulated luminescence dates from MAL05-1C are inaccurate for sediment older than ∼50 ka. Between 20 and 30 MBLF, the revised age–depth model yields a higher average sedimentation rate of ∼0.03 cm/year, consistent with the upper part of the core, which was dated extensively by radiocarbon (24). The stratigraphic position of key climatic "events" within the Lake Malawi sediments can now be more accurately pinpointed; for example, the hypothesized 75 ka human bottleneck (10) moves from ∼37 MBLF to ∼28 MBLF in MAL05-1C. Other features of the record are also redated, such as the East African megadroughts (24), which must have terminated at least 10 ka earlier than the previous estimate of 75 ka B.P. Clearly, existing comparisons of the Lake Malawi paleoclimate data to other regional and global records (24, 25, 32) will need to be revised in the light of these findings. If YTT can be located in other African paleoclimate archives, this valuable isochron will facilitate more precise comparisons between records that currently have poor age control beyond the limits of radiocarbon dating (>50 ka B.P.).

The sediments of Lake Malawi contain YTT cryptotephra within an undisturbed, thin-bedded interval. The first deposition of the YTT is well constrained to within 1 cm (Fig. 2), equivalent to ∼30 y (*Materials and Methods*). The sharp base of the tephra profile in Fig. 2*A* indicates deposition from an airfall event. Inwashed ash from the lake catchment may also have reached the core location; however, ash concentrations drop dramatically after 2 cm (∼60 y). With less than 3,500 glass shards per gram of sediment found within 1 cm depth of core, we estimate that the ash would not have formed a visible layer over the Malawi catchment. The direct impact of such a low concentration of fine-

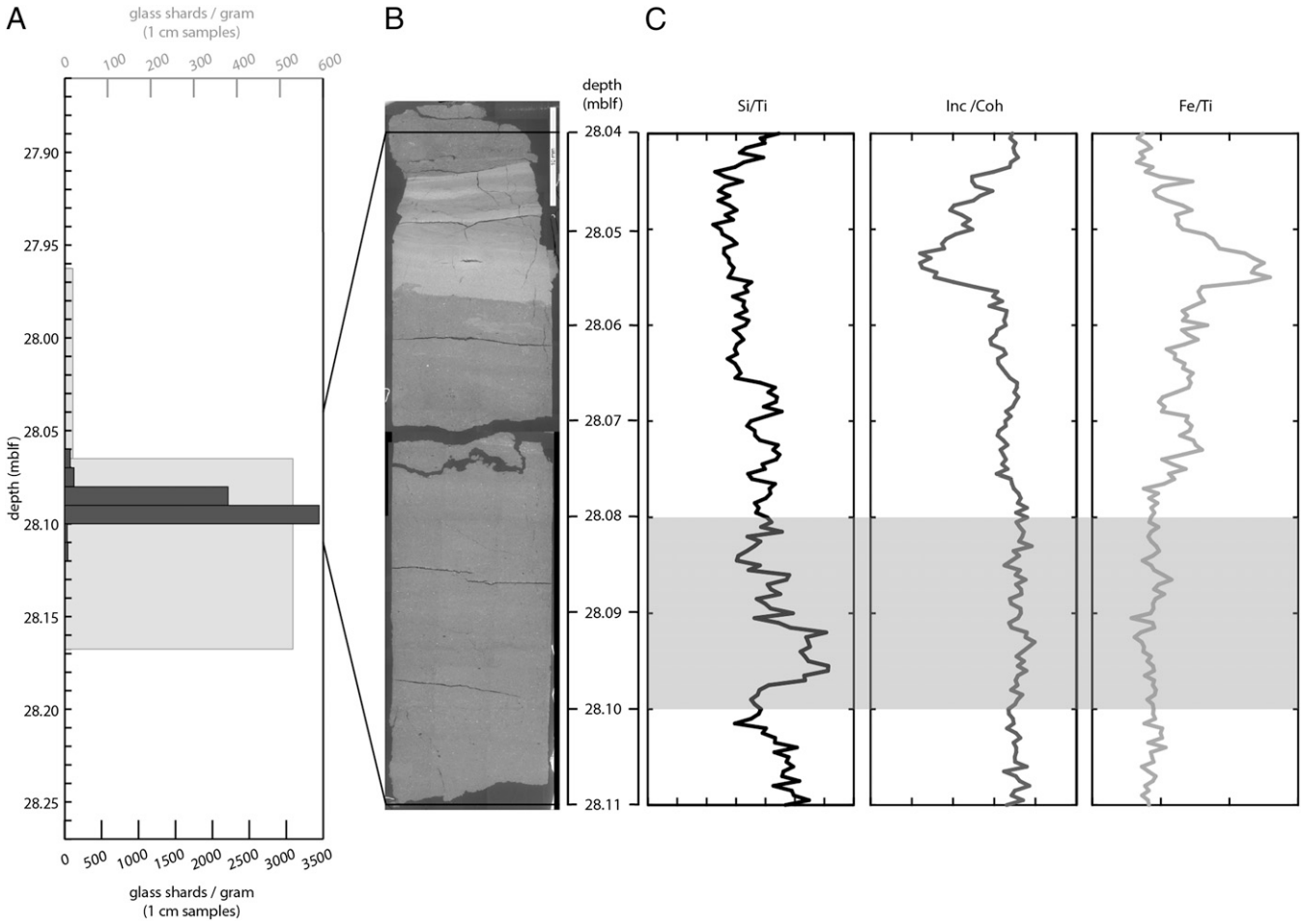

Fig. 2. The position of the YTT cryptotephra layer in MAL05-1C and sediment composition data. (*A*) The distribution of YTT glass shards in GLAD-MAL05-1C. The number of volcanic glass shards (shards/gram of sediment) was counted in 10-cm (gray bars) then 1-cm (black bars) depth samples. A peak in concentration is visible at 28.10 MBLF. (*B*) The YTT cryptotephra layer is not visible in a SEM image (backscatter electron mode) of a thin section from the core between 28.04 and 28.11 MBLF; however, the image confirms the lack of bioturbation or disturbance in the core at this depth and is evidence for anoxic bottom water conditions at this time. The white layer above 28.06 MBLF is a turbidite layer not related to the YTT. (*C*) Scanning XRF data across the same interval also shows no significant perturbations in either composition or coherence of the sediment. Gray shading denotes the 2 cm of sediment containing YTT shards, 28.10–28.08 MBLF.

grained ash on the local ecosystem during half a century would have been negligible. We microscopically examined smear slides of sediment at a 2-mm interval from below, within, and above the YTT horizon in Malawi core MAL05-1C. The sediments are *Aulacoseira*-dominated diatomaceous silty clay and display no obvious change in composition throughout the 4-cm interval (28.07–28.11 MBLF). An X-ray fluorescence (XRF) scan of the interval displays a slight rise in the ratio of Si/Ti, an indication of slightly elevated diatom productivity (33), but no change in other parameters, such as sulfur content, in the ratio of Fe/Ti (suggesting no major shift in redox conditions in the lake), or in the ratio of incoherent to coherent signal strength, which reflects the abundance of organic matter in Lake Malawi sediment (33) (Fig. 2). Lake Malawi is presently anoxic below 200 m depth, and it was likely in this state at the time of the eruption of Toba. Had regional temperature cooled by ∼4 °C, as has been estimated from climate models of the eruption's impact (14), the lake would likely have experienced massive overturn of the water column, a major iron oxidation event, and extermination of much of the biota in the upper water column. The sediments in core 1C display no clear evidence for such a catastrophic event.

Paleotemperature reconstructions using the TEX_{86} organic biomarker display no unusual response to the Toba eruption. A previously published paleotemperature record of core MAL05-2A was carried out at a resolution of ∼1,000 y (32). We analyzed the Toba horizon and four additional depths in MAL05-2A for TEX_{86} and found the Toba interval records a temperature drop of ∼1.5 °C relative to sediment above and below this horizon (Fig. S1). This cooling is less severe than what is observed in other parts of the MAL05-2A record. We conclude that the hypothesized "volcanic winter" that followed the Toba eruption did not have a significant impact on the climate of East Africa and was not the cause of a human bottleneck in Africa around 75 ka B.P.

Materials and Methods

Cryptotephra layers were detected using standard physical separation methods (34). Contiguous and continuous 10-cm samples were treated with 1 mol/L HCl, sieved (>25 μm) and density separated (1.95–2.55 g·cm^{-3}) to isolate volcanic glass shards, which were counted under high-power microscopy. Intervals of >20 shards per gram were resampled and reprocessed to locate the cryptotephra layer to within 1-cm depth. Tephra shards were mounted on a 25-mm epoxy resin stub and polished to expose internal surfaces for analysis by electron microprobe.

Single-grain major and minor element compositions were measured using electron microprobe wavelength dispersive spectrometry at the University of Oxford Research Laboratory for Archaeology and the History of Art, using a Jeol JXA8600 electron microprobe, in wavelength dispersive mode, with

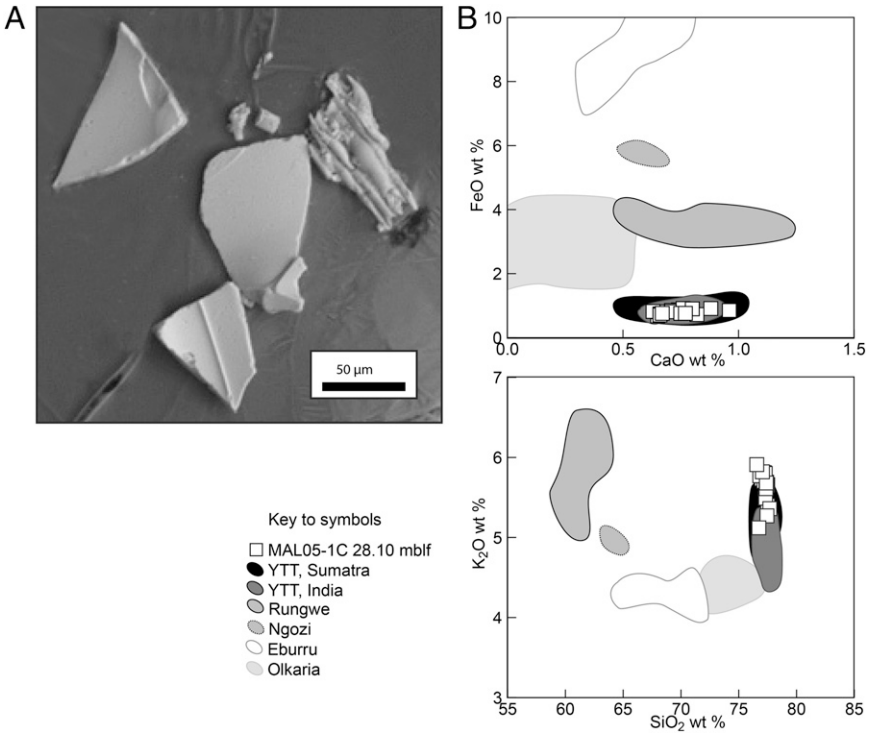

Fig. 3. Chemical and visual characteristics of YTT glass shards. (*A*) SEM image of glass shards from the YTT layer in MAL05-1C. Note the dominance of platy, bubble wall shards as well as one with some elongate vesicles (*Right*). (*B*) Chemical correlation of glass shards from cryptotephra layer in MAL05-1C (28.10 MBLF) with both proximal (Sumatra) and distal (India) deposits of the YTT (29). Glass compositions of the YTT (open squares) are clearly distinct from tephra of the Rungwe Volcanic Province (26) and of the Olkaria (27) and Eburru (28) volcanoes, Kenya, which have produced rhyolitic eruptions during the last 150 ka. Uncertainty for data generated in this study, calculated from 2 SD precision of secondary standard analyses, is contained within the YTT symbols.

15-keV accelerating voltage, 6-nA beam current, and 10-µm defocused beam. On-peak count times were 10 s for Na; 30 s for Si, Al, K, Ca, Fe, Mg, Ti, and Mn; and 60 s for P. The electron probe was calibrated using a suite of characterized minerals and oxides standards; accuracy and precision was monitored by intermittent analysis of fused volcanic glass standards ATHO-G and StHs6/80-G, from the Max-Planck-Institut für Chemie–Dingwell (MPI-DING) collection (35, 36) (Table S1).

The revised age model for the top 30 m of MAL05-1C (Fig. 4) was generated using 15 radiocarbon ages (7) and the latest high-precision YTT age estimate of 75.0 ± 0.9 ka (4) in a Bayesian *P-Sequence* depositional model (37), run in OxCal version 4.1 (38) with outlier analysis (39) and interpolation at 0.5 m intervals. Radiocarbon dates were calibrated using the IntCal09 curve (40). The approximate sedimentation rate of 0.03 cm·year^{-1} stated in the text for the time interval around the YTT deposition was calculated directly from our age model, using the interval 20–30 m. Across this interval, the model has a 2-sigma uncertainty of between 2% and 10%.

The analytical methods used to determine TEX_{86} were identical to those described elsewhere (32).

Table 1. Chemical composition of YTT glass shards in Lake Malawi, compared with proximal samples from the Toba caldera in Sumatra, Indonesia and YTT ash from the Indian archaeological site of Jwalapuram (29)

Sample	SiO_2	TiO_2	Al_2O_3	FeO	MnO	MgO	CaO	Na_2O	K_2O	Total*
Cryptotephra layer, MAL05-1C 28.10 MBLF										
Average (n = 18)	77.24	0.05	12.41	0.84	0.07	0.05	0.77	2.95	5.61	100
2 SD	1.79	0.04	0.31	0.14	0.08	0.06	0.19	0.37	0.45	
Cryptotephra layer, MAL05-2a 26.78 MBLF										
Average (n = 9)	77.22	0.04	12.32	0.84	0.07	0.05	0.78	3.2	5.47	100
2 SD	0.47	0.05	0.27	0.11	0.05	0.03	0.21	0.26	0.26	
YTT, Toba caldera										
Average (n = 118)	77.24	0.06	12.54	0.85	0.07	0.05	0.78	3.10	5.20	100
2 SD	0.7	0.06	0.39	0.24	0.09	0.04	0.21	0.34	0.29	
YTT, Jwalapuram, India										
Average (n = 113)	77.36	0.06	12.49	0.87	0.07	0.07	0.75	3.25	4.93	100
2 SD	0.28	0.02	0.2	0.09	0.04	0.1	0.78	0.16	0.16	

*All data normalized to water free compositions. Table S1 contains the full dataset and associated secondary standard analyses. For details of analytical conditions, see *Materials and Methods*.

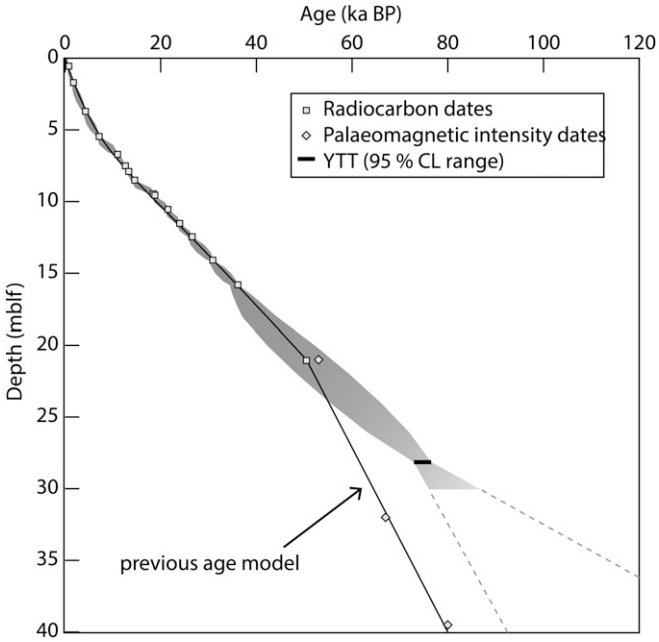

Fig. 4. The revised age-depth model for MAL05-1C. A revised Bayesian age-depth model for the upper 30 m of MAL05-1C based on 15 radiocarbon dates (24) and the age of the YTT: 75 ± 0.9 ka B.P. (4). Gray shading denotes modeled 95% confidence intervals. Beyond 30 m depth, no secure independent age estimates are available and a tentative age–depth relationship is projected to 40 m assuming linear sedimentation (dashed lines). The previous MAL05-1C age model (24) is shown for comparison. For details of model construction, see *Materials and Methods*.

ACKNOWLEDGMENTS. We thank V. C. Smith at the University of Oxford for electron probe microanalysis; the coprincipal investigators of the Lake Malawi Drilling Project (C. A. Scholz, A. S. Cohen, and J. King) and other members of the drilling team; A. Noren and A. Myrbo (LacCore) for assistance with sampling; T. Shanahan for producing a thin section of the Toba interval; A. Lingwall and E. T. Brown for assistance with scanning XRF; J. Halbur for TEX_{86} analyses; and B. Bandli for SEM images. A. S. Cohen and A. M. Pollard provided useful suggestions for improvement of the manuscript. This research was funded in part by National Science Foundation Grant EAR 0902714 (to T.C.J.) and by the Leverhulme Trust (C.S.L.).

1. Rose WI, Chesner CA (1990) Worldwide dispersal of ash and gases from earth's largest known eruption: Toba, Sumatra, 75 ka. *Palaeogeogr Palaeoclimatol Palaeoecol* 89(3):269–275.
2. Robock A (2001) Volcanic eruptions and climate. *Rev Geophys* 38(2):191–219.
3. Huang CH, Zhao M, Wang CW, Wei G (2001) Cooling of the South China Sea by the Toba eruption and correlation with other climate proxies ~71,000 years ago. *Geophys Res Lett* 28(20):3915–3918.
4. Mark DF, et al. A high-precision 40Ar/39Ar age for the Young Toba Tuff and dating of ultra-distal tephra: Forcing of Quaternary climate and implications for hominin occupation of India. *Quat Geochronol*, 10.1016/j.quageo.2012.12.004.
5. Ninkovich D, Sparks RSJ, Ledbetter MT (1978) The exceptional magnitude and intensity of the Toba eruption, Sumatra: An example of the use of deep-sea tephra layers as a geological tool. *Bulletin Volcanologique* 41(3):286–298.
6. Pattan JN, Shane P, Banakar VK (1999) New occurrence of Youngest Toba Tuff in abyssal sediments of the Central Indian Basin. *Mar Geol* 155(3–4):243–248.
7. Schulz H, Emeis KC, Erlenkeuser H, von Rad U, Rolf C (2002) The Toba volcanic event and interstadial/stadial climates at the marine isotopic stage 5 to 4 transition in the Northern Indian Ocean. *Quat Res* 57(1):22–31.
8. Shane P, Westgate J, Williams M, Korisettar R (1995) New geochemical evidence for the Youngest Toba Tuff in India. *Quat Res* 44(2):200–204.
9. Timmreck C, et al. (2010) Aerosol size confines climate response to volcanic supereruptions. *Geophys Res Lett* 37(L24705).
10. Ambrose SH (1998) Late Pleistocene human population bottlenecks, volcanic winter, and differentiation of modern humans. *J Hum Evol* 34(6):623–651.
11. Rampino MR, Ambrose SH (2000) Volcanic winter in the Garden of Eden: The Toba supereruption and the late Pleistocene human population crash. Volcanic Hazards and Disasters in Human Antiquity, eds McCoy FW, et al. *GSA Special Papers* 345: 71–82.
12. Petraglia M, et al. (2007) Middle Paleolithic assemblages from the Indian subcontinent before and after the Toba super-eruption. *Science* 317(5834):114–116.
13. Gathorne-Hardy FJ, Harcourt-Smith WEH (2003) The super-eruption of Toba, did it cause a human bottleneck? *J Hum Evol* 45(3):227–230.
14. Timmreck C, et al. (2012) Climate response to the Toba super-eruption: Regional changes. *Quat Int* 258:30–44.
15. Williams M (2012) Did the 73 ka Toba super-eruption have an enduring effect? Insights from genetics, prehistoric archaeology, pollen analysis, stable isotope geochemistry, geomorphology, ice cores, and climate models. *Quat Int* 269:87–93.
16. Zielinski GA, et al. (1996) Potential atmospheric impact of the Toba mega-eruption ~71,000 years ago. *Geophys Res Lett* 23(8):837–840.
17. Storey M, Roberts RG, Saidin M (2012) Astronomically calibrated 40Ar/39Ar age for the Toba supereruption and global synchronization of late Quaternary records. *Proc Natl Acad Sci USA* 109(46):18684–18688.
18. Svensson A, et al. (2012) Direct linking of Greenland and Antarctic ice cores at the Toba eruption (74 kyr BP). *Clim. Past Discuss.* 8:5389–5427.
19. Haslam M, Petraglia M (2010) Comment on "Environmental impact of the 73ka Toba super-eruption in South Asia" by Williams, MAJ, Ambrose, SH, van der Kaars, S, Ruehlemann, C, Chattopadhyaya, U, Pal J, Chauhan, PR (2009) [Paleogeogr Paleoclimatol Paleoecol 284:295-314]. *Paleogeogr Paleoclimatol Paleoecol* 296:199–203.
20. Rampino MR, Self S, Stothers RB (1988) Volcanic winters. *Annu Rev Earth Planet Sci* 16:73–99.
21. Premo LS, Hublin JJ (2009) Culture, population structure, and low genetic diversity in Pleistocene hominins. *Proc Natl Acad Sci USA* 106(1):33–37.
22. Armitage SJ, et al. (2011) The southern route ''Out of Africa''. Evidence for an Early Expansion of Modern Humans into Arabia. *Science* 331(6016):453.
23. Williams MAJ, et al. (2009) Environmental impact of the 73 ka Toba super-eruption in South Asia. *Palaeogeogr Palaeoclimatol Palaeoecol* 284:295–314.
24. Scholz CA, et al. (2007) East African megadroughts between 135 and 75 thousand years ago and bearing on early-modern human origins. *Proc Natl Acad Sci USA* 104(42):16416–16421.
25. Scholz CA, et al. (2011) Scientific drilling in the Great Rift Valley: The 2005 Lake Malawi Scientific Drilling Project — An overview of the past 145,000 years of climate variability in Southern Hemisphere East Africa. *Palaeogeogr Palaeoclimatol Palaeoecol* 303:3–19.
26. Fontijn K, et al. (2010) Holocene explosive eruptions in the Rungwe Volcanic Province, Tanzania. *J Volcanol Geotherm Res* 196(1–2):91–110.
27. Marshall AS, et al. (2009) Fractionation of peralkaline silicic magmas: The greater olkaria volcanic complex, Kenya Rift Valley. *J Petrol* 50(2):323–359.
28. Ren M, et al. (2006) Application of the QUILF thermobarometer to the peralkaline trachytes and pantellerites of the Eburru volcanic complex, East African Rift, Kenya. *Lithos* 91(1–4):109–124.
29. Smith VC, et al. (2011) Geochemical fingerprinting of the widespread Toba tephra using biotite compositions. *Quat Int* 246:97–104.
30. Matthews NE, et al. (2012) Ultra-distal tephra deposits from super-eruptions: Examples from Toba, Indonesia and Taupo Volcanic Zone, New Zealand. *Quat Int* 258: 54–79.
31. Renne PR, Mundil R, Balco G, Min K, Ludwig KR (2010) Joint determination of 40K decay constants and 40Ar/40K for the Fish Canyon sanidine standard, and improved accuracy for 40Ar/39Ar geochronology. *Geochim Cosmochim Acta* 74:5349–5367.
32. Woltering M, Johnson TC, Werne JP, Schouten S, Sinninghe Damsté JS (2011) Late Pleistocene temperature history of Southeast Africa: A TEX86 temperature record from Lake Malawi. *Palaeogeogr Palaeoclimatol Palaeoecol* 303:93–102.
33. Brown ET, Johnson TC, Scholz CA, Cohen AS, King JW (2007) Abrupt change in tropical African climate linked to the bipolar seesaw over the past 55,000 years. *Geophys Res Lett* 34:L20702.
34. Blockley SPE, et al. (2005) A new and less destructive laboratory procedure for the physical separation of distal glass tephra shards from sediments. *Quat Sci Rev* 24(16–17):1952–1960.
35. Jochum KP, et al. (2006) MPI-DING reference glasses for in situ microanalysis: New reference values for element concentrations and isotope ratios. *Geochem Geophys Geosyst* 7(Q02008).
36. Jochum KP, et al. (2005) GeoReM: A new geochemical database for reference materials and isotopic standards. *Geostandards and Geoanalytical Research* 29(3):333–338.
37. Ramsey CB (2008) Deposition models for chronological records. *Quat Sci Rev* 27(1–2): 42–60.
38. Bronk Ramsey C (2001) Development of the Radiocarbon Program OxCal. *Radiocarbon* 43(2A):355–363.
39. Ramsey CB (2009) Dealing with outliers and offsets in radiocarbon dating. *Radiocarbon* 51(3):1023–1045.
40. Reimer PJ, et al. (2009) INTCAL09 and MARINE09 radiocarbon age calibration curves, 0-50,000 years cal BP. *Radiocarbon* 51(4):1111–1150.

Supporting Information

Lane et al. 10.1073/pnas.1301474110

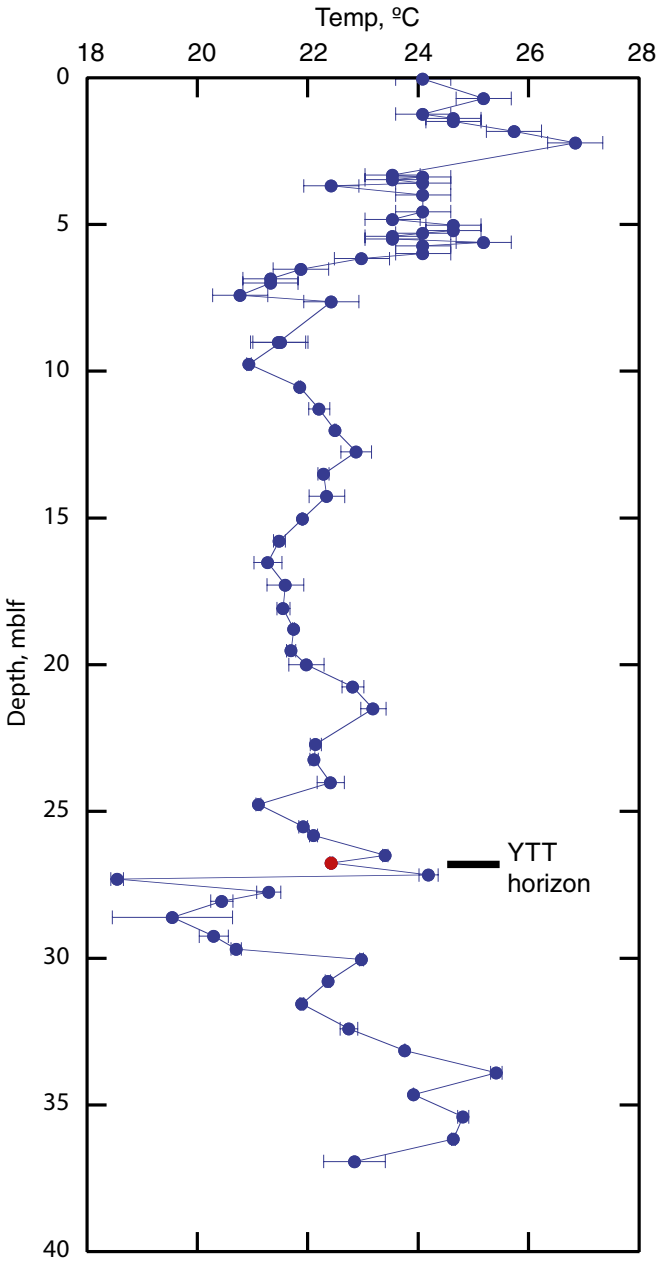

Fig. S1. Lake Malawi surface water temperature history based on the TEX_{86} organic biomarker analyses of sediment in piston core M98-2P [0–12 m below lake floor (MBLF)] and in drill core MAL05-2A (10–40 MBLF). Error bars reflect SDs on duplicate analyses. The temperature derived from the Toba horizon is depicted in red.

Table S1. Geochemical analysis of the YTT

Sample	SiO_2	TiO_2	Al_2O_3	FeO	MnO	MgO	CaO	Na_2O	K_2O	P_2O_5	Total
Cryptotephra layer, MAL05-1C 28.10 MBLF											
1	74.98	0.01	11.90	0.68	0.07	0.05	0.65	3.16	5.22	0.02	95.34
2	74.34	0.02	12.13	0.87	0.00	0.07	0.74	2.73	5.28	0.00	94.67
3	74.37	0.07	11.97	0.85	0.08	0.04	0.71	2.51	5.47	0.00	95.13
4	74.24	0.04	11.80	0.77	0.09	0.01	0.66	2.75	5.42	0.00	95.28
5	73.77	0.08	11.76	0.91	0.14	0.03	0.76	2.90	5.49	0.00	95.80
6	74.08	0.05	11.90	0.81	0.03	0.05	0.70	2.93	5.26	0.00	95.84
7	73.91	0.06	11.79	0.81	0.02	0.07	0.65	2.72	5.39	0.00	95.15
8	74.08	0.02	11.78	0.82	0.13	0.01	0.63	2.76	5.11	0.01	96.74
9	73.61	0.05	11.75	0.83	0.08	0.01	0.80	2.67	5.54	0.00	94.91
10	73.53	0.07	11.87	0.72	0.06	0.05	0.82	2.72	5.43	0.00	94.97
11	73.61	0.05	11.74	0.76	0.00	0.07	0.75	2.85	5.34	0.00	95.10
12	73.53	0.07	11.72	0.74	0.04	0.03	0.66	2.83	5.51	0.00	95.36
13	73.65	0.05	11.76	0.71	0.07	0.05	0.66	3.16	5.01	0.00	95.81
14	72.96	0.04	11.92	0.90	0.06	0.07	0.80	2.69	5.48	0.05	96.18
15	72.84	0.07	12.03	0.85	0.06	0.10	0.96	3.15	4.86	0.00	96.07
16	73.26	0.07	11.62	0.76	0.07	0.06	0.67	2.76	5.37	0.02	94.42
17	72.75	0.04	11.85	0.76	0.05	0.03	0.77	2.65	5.50	0.02	93.94
18	71.92	0.05	11.68	0.91	0.10	0.10	0.88	2.72	5.55	0.03	95.42
Cryptotephra layer, MAL05-2a 26.78 MBLF											
1	73.16	0.04	11.82	0.84	0.05	0.04	0.84	3.09	5.01	0.00	94.90
2	74.05	0.05	11.58	0.83	0.05	0.06	0.70	2.91	5.10	0.02	95.34
3	73.01	0.00	11.77	0.73	0.11	0.03	0.58	3.09	5.20	0.01	94.52
4	72.70	0.03	11.51	0.72	0.07	0.07	0.80	2.81	5.26	0.00	93.98
5	73.43	0.07	11.62	0.78	0.10	0.04	0.68	3.07	5.42	0.00	95.22
6	73.71	0.02	11.75	0.86	0.03	0.06	0.66	3.13	5.11	0.03	95.35
7	72.98	0.06	11.93	0.79	0.07	0.03	0.89	3.08	5.19	0.01	95.03
8	72.93	0.05	11.64	0.85	0.08	0.07	0.81	2.90	5.18	0.03	94.53
9	73.12	0.02	11.58	0.74	0.06	0.04	0.69	3.21	5.20	0.06	94.72
Secondary standard glasses											
ATHO-G											
Average (n = 13)	75.31	0.25	12.19	3.17	0.11	0.08	1.68	4.09	2.78	0.02	
2σ	0.49	0.06	0.26	0.19	0.10	0.02	0.07	0.21	0.07	0.04	
Preferred value	75.60	0.26	12.20	3.27	0.11	0.10	1.70	3.75	2.64	0.03	
Uncertainty (95% CI)	0.70	0.02	0.20	0.10	0.01	0.01	0.03	0.31	0.09	0.00	
StHs6/80-G											
Average (n = 14)	63.68	0.72	17.66	4.35	0.07	1.96	5.34	4.54	1.31	0.18	
2σ	0.43	0.09	0.31	0.26	0.09	0.09	0.15	0.63	0.06	0.06	
Preferred value	63.70	0.70	17.80	4.37	0.08	1.97	5.28	4.44	1.29	0.16	
Uncertainty (95% CI)	0.50	0.02	0.20	0.07	0.00	0.04	0.09	0.14	0.02	0.02	

Major and minor element (unnormalized weight % oxide) compositions of glass shards from the YTT in Malawi and associated secondary standard glasses (1). Preferred values for the MPI-DING secondary standards (ATHO-G and StHs6/80-G) are taken from the GeoRem online database (2). MBLF, meters below lake floor; YTT, Youngest Toba Tuff.

1. Jochum KP, et al. (2006) MPI-DING reference glasses for in situ microanalysis: New reference values for element concentrations and isotope ratios. *Geochem Geophys Geosyst* 7(Q02008).
2. Jochum KP, et al. (2005) GeoReM: A new geochemical database for reference materials and isotopic standards. *Geostandards and Geoanalytical Research* 29(3):333–338.